Crystal structure of Rab9 complexed to GDP reveals a dimer with an active conformation of switch II

Julia G. Wittmann, Markus G. Rudolph*

Department of Molecular Structural Biology and GZMB, Justus-von-Liebig-Weg 11, Georg-August University, 37077 Göttingen, Germany

Received 21 April 2004; revised 3 May 2004; accepted 4 May 2004

Available online 13 May 2004

Edited by Hans Eklund

Abstract The small GTPase Rab9 is an essential regulator of vesicular transport from the late endosome to the trans-Golgi network, as monitored by the redirection of the mannose-6-phosphate receptors. The crystal structure of Rab9 complexed to GDP, Mg^{2+}, and Sr^{2+} reveals a unique dimer formed by an intermolecular -sheet that buries the switch I regions. Surface area and shape complementarity calculations suggest that Rab9 dimers can form an inactive, membrane-bound pool of Rab9 · GDP that is independent of GDI. Mg^{2+}-bound Rab9 represents an inactive state, but Sr^{2+}-bound Rab9 · GDP displays activated switch region conformations, mimicking those of the GTP state. A hydrophobic tetrad is formed resembling an effector-discriminating epitope found only in GTP-bound Rab proteins.

Keywords: Ras-like GTPase; Intracellular transport; Protein–protein interaction; Crystal structure; Merohedral twinning

1. Introduction

A distinguishing feature of eukaryotic cells is the compartmentalization of their interior into membrane-delimited organelles. Communication between these compartments is mediated by transport vesicles, which bud from a donor membrane, are transported to a target organelle in a vectorial fashion, and fuse with their acceptor membrane. The vesicular transport machinery [1,2] is tightly regulated by the Rab/Ypt group of Ras-related small GTP-binding proteins.

Ras-related proteins share common properties: they are small (20–25 kDa), monomeric, P-loop-containing GDP/GTP-binding proteins that control a plethora of cellular processes such as signal transduction, cell proliferation, actin cytoskeletal reorganization, nuclear import and vesicular transport [3]. As molecular switches, they cycle between an inactive, GDP-bound, and an active, GTP-bound, state that interacts with its downstream effectors. The main determinants for effector recognition are the switch I and switch II regions, which undergo large conformational changes upon GTP binding. The ratio of the GDP- and GTP-bound states is regulated by guanine nucleotide exchange factors (GEFs), which populate the GTP-bound form, and GTPase activating proteins (GAPs), which accelerate the slow intrinsic GTP-hydrolysis rate by a factor of up to 10^5-fold [4], thereby populating the inactive form.

Within the superfamily of Ras-like GTP-binding proteins, the Rab/Ypt proteins represent the largest family with 11 homologues described in yeast (termed Ypt) and about 50 mammalian Rab homologues described to date [5]. Rab/Ypt proteins play key roles in vesicular transport processes such as endo- and exocytosis, as well as trafficking between intracellular compartments. The necessity to precisely regulate the multitude of Rab/Ypt activities is exemplified by the fact that, in addition to GEFs and GAPs, Rab proteins are regulated by an additional set of proteins such as guanine nucleotide dissociation inhibitor (GDI) and Rab escort protein (REP), and there is no cross-talk between the different sets of effector molecules. In addition to the switch regions, Rab proteins employ sequences at their termini and the α_3/β_5 loop, termed complementary determining regions (CDRs) [6], to bind their effectors. The slight sequence and structural variation of these CDRs within the Rab proteins are thought to be the main features with which Rab proteins specifically recognize their effectors.

Rab9 plays a pivotal role in regulating vesicular transport from late endosomes to the trans-Golgi network (TGN) by redirecting mannose-6-phosphate receptors (MPRs) and, accordingly, is predominantly localized at late endosomal membranes [7]. During anterograde (Golgi to TGN) transport, adaptor proteins such as AP-1 and GGAs bind to the cytoplasmic tails of MPRs to recruit their cargo proteins into clathrin-coated vesicles [8,9]. After fusion of these vesicles with endosomes, the MPRs release their cargo and are recycled to the TGN to enter a new round of transport. This retrograde transport of MPRs was found to be regulated by a novel adaptor protein (tail interacting protein of 47 kDa, TIP47) [10]. Rab9 has been shown to interact with TIP47 in a nucleotide-dependent fashion, recruiting TIP47 to a endosomal membrane. Thus, Rab9 · GTP, TIP47 and MPRs should form a stable ternary complex [5].

While several crystal structures are available for components of the anterograde MPR trafficking machinery [11], no structures have been reported for any component involved in retrograde MPR recycling. Thus, we set out to determine the crystal structure of the important regulatory GTPase Rab9 to establish a structural basis for this important receptor

* Corresponding author. Fax: +49-551-39-14082.
E-mail address: markus.rudolph@bio.uni-goettingen.de (M.G. Rudolph).

Abbreviations: CDR, complementary determining region; GAP, GTPase activating protein; GDI, guanine nucleotide dissociation inhibitor; GEF, guanine nucleotide exchange factor; MPRs, mannose-6-phosphate receptors; REP, Rab escort protein; TGN, trans-Golgi network; TIP47, tail interacting protein of 47 kDa

0014-5793/$22.00
doi:10.1016/j.febslet.2004.05.004

trafficking pathway. Here, we present the structure of Rab9 in complex with GDP at a resolution of 1.77 Å. There are two molecules in the asymmetric unit forming a unique dimeric structure. Each monomer is complexed to a different metal ion, i.e., Mg^{2+} and Sr^{2+}, leading to an active conformation of switch II in one molecule. Most parts of the switch I and switch II regions, which normally are disordered in structures of GDP-bound Ras-like GTPases, show clear electron density. The CDRs are also ordered but show elevated temperature factors, consistent with their role as binding sites for Rab effectors. The Rab9 structure is discussed in light of the related Rab homologues, Ypt7p and Rab11a.

2. Materials and methods

2.1. Expression, purification, and crystallization of the Rab9 · GDP complex

Cloning, protein production and crystallization of the Rab9 · GDP complex have been described elsewhere [12]. Trigonal crystals of Rab9 · GDP grew from solutions containing a 1:1 mixture of Rab9 and 18.5% PEG8000, 0.1M MES/NaOH, pH 6.0, 0.2 M sodium benzoate, 2% ethanol, and 5 mM $MgCl_2$. Addition of 8 mM $SrCl_2$ to the crystallization setup changed the space group from trigonal $P3_\gamma$ to tetragonal $I4_1$ and at the same time improved the diffraction limit from 3 to <2 Å. Both crystal forms displayed hemihedral twinning with twin fractions between 0.25 and 0.50. Due to the mediocre diffraction of the trigonal crystals compared to the tetragonal crystals, the trigonal space group was not further analyzed.

Table 1
Data processing, molecular replacement, and refinement statistics

Data processing	
Space group	$I4_1$
Cell (a, c) (Å)	98.25, 79.66
Resolution range (outer shell)[a] (Å)	34.7–1.77 (1.83–1.77)
# Unique reflections	37 662 (3752)
Completeness (%)	99.9 (99.9)
R_{sym} (%)[b]	5.3 (69.1)
Average I/σ (I)	24.8 (2.5)
Multiplicity of observations	3.8 (3.8)
Mosaicity (°)	0.25
Mean $\lvert E^2 - 1\rvert$	0.622 (0.736)[c]
Molecular replacement	
Resolution range (Å)	14–4
Rotation function (I/σ)	4.6/4.4 (next false peak: 4.1)
Translation function (CC, R)	35.1/45.2
Rigid body refinement (CC)	37.9
Refinement	
Resolution range (Å)	30.0–1.77
R_{cryst}[d] (%)	16.5
R_{free} (%)	22.1
Refined twin fraction	0.253
# Protein atoms/waters/others	2712/231/96
Coordinate error (Å)[e]	0.29
Rms deviation from ideality	
Bonds (Å)/angles (°)/dihedrals (°)	0.007/2.1/25.5
Ramachandran plot[f]	
Favored, allowed, generous (%)	89.8/9.8/0.3
Average temperature factors (Å^2)	
Molecule A/GDP/Sr^{2+}	27.5/22.7/29.2
Molecule B/GDP/Mg^{2+}	31.7/31.0/20.4
Waters/benzoic acid/Cl^-	35.8/23.2/37.5

[a] Numbers in parentheses refer to the highest resolution shell.
[b] $R_{sym} = 100 \cdot \sum_h \sum_i |I_i(h) - \langle I(h)\rangle| / \sum_h I(h)$, where $I_i(h)$ is the ith measurement of reflection h of average reflection intensity $\langle I(h)\rangle$.
[c] Calculated with XPREP (Bruker, Axs). Value in parentheses is the expected value for a non-twinned chiral specimen.
[d] $R_{cryst} = 100 \cdot \sum ||F_o| - |F_c|| / \sum |F_o|$, where F_o and F_c are the structure factor amplitudes from the data and the model, respectively. R_{free} is R_{cryst} with 5% of test set structure factors.
[e] Coordinate error based on a Luzzati plot [52].
[f] Calculated using PROCHECK [23].

2.2. Data collection, structure determination, and model analysis

Data were collected on flash-cooled crystals and reduced with the DENZO/SCALEPACK suite [13]. A slightly twinned ($\alpha = 0.3$) dataset was collected on a rotating anode to a resolution of 2.3 Å and used for molecular replacement trials with COMO [14] without taking twinning into account. The Ypt7p complex [15] (PDB-ID 1KY3), with nucleotide, switch regions, and water coordinates removed, was used as a search model. The correct molecular replacement solution comprises two molecules related by a twofold axis, which aligns with an axis described by a symmetry operator of the 4/mmm Laue group to introduce pseudo-422 symmetry. This additional symmetry allows for hemihedral twinning with the twin operator being $(k, h, -l)$. First phases were generated from this solution but the electron density maps were not interpretable. Density modification using DM [16], including NCS averaging and phase extension from 6 to 2.3 Å, yielded high quality σ_A-weighted $3F_o - 2F_c$ and $F_o - F_c$ difference electron density maps [17], into which >90% of the Rab9 model was fitted using O [18]. At this stage a high resolution dataset to 1.77 Å with a twin fraction of ca. 0.25 was collected at beamline BW7A of the Deutsche Elektronensynchrotron (DESY) and used for refinement of the Rab9 · GDP complex in CNS [19] and SHELXL [20]. A random set of 5% of reflections was excluded from refinement to monitor R_{free} [21]. Water molecules were assigned for $>3\sigma$ peaks in $F_o - F_c$ difference maps, and retained if they obeyed hydrogen bonding criteria according to HBPLUS [22] and returned $>1.2\sigma$ density after refinement. The refinement statistics are summarized in Table 1. The final model includes residues 5–111 and 114–174 for molecule A and residues 1–33 and 36–173 for molecule B. The quality of the model was analyzed using the programs PROCHECK [23] and WHATCHECK [24] (Table 1). Figures were created with Bobscript [25] and rendered with Raster3D [26].

3. Results and discussion

3.1. Protein design and structure determination using twinned crystals

With the exception of Cdc42 [27], structures of Ras-related GTPases either lack the C-terminal part or they do not display interpretable electron density. The flexible C-terminus, which in vivo often is post-translationally farnesylated or geranylgeranylated for membrane attachment, appears to negatively affect crystallization. Consistently, crystallization attempts using the full-length Rab9 were unsuccessful. Thus, a C-terminally truncated Rab9 fragment was generated consisting of residues 1–175 [12]. Twinned trigonal and tetragonal crystal forms suitable for data collection were grown using the truncated Rab9. The tetragonal crystal form diffracted X-rays to high resolution and was used for structure determination by molecular replacement using the yeast Rab7 homologue Ypt7p [15] as the starting model. The Rab9 structure was refined to a resolution of 1.77 Å against twinned intensities using SHELXL [20], yielding an R_{free} value of 22.1% (Table 1). The final model displays excellent stereochemistry and includes two molecules of Rab9. These molecules differ from each other considerably and were refined and are discussed independently.

3.2. Overall structure of Rab9

The overall structure of the monomeric Rab9 · GDP complex shares the fold of the Ras-like GTP-binding proteins (Figs. 1 and 2A), and consists of a six stranded β-sheet (β1–β6) surrounded by five α helices (α1–α5) and two 3_{10}-helical seg-

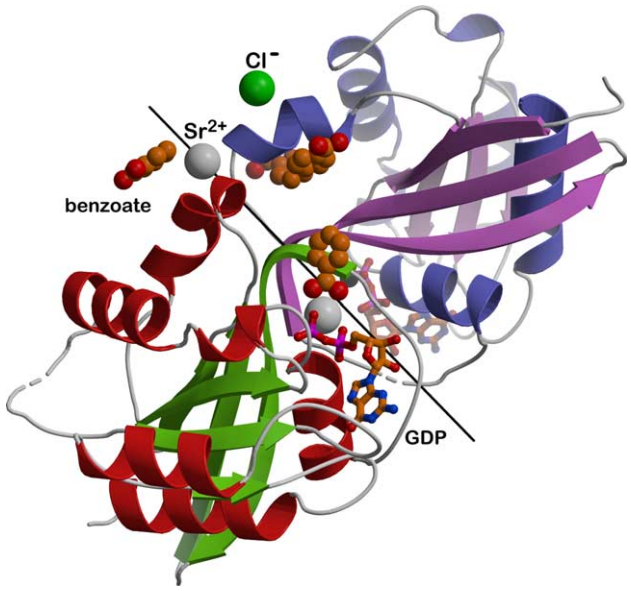

Fig. 1. The Rab9 dimer. The Rab9 asymmetric unit is shown as a ribbon diagram. Molecule A is colored in red (helices) and green (β-strands), molecule B is shown in blue (helices) and pink (β-strands), and coil regions are colored in gray. The nucleotides are drawn as ball-and-stick models and colored according to atom type. Sr^{2+}, Mg^{2+}, and Cl^- ions are represented as gray, dark gray, and green spheres, respectively, and the benzoate moieties are drawn as cpk-models. Discontinuities in the structure are marked as dashed lines.

ments (η1 and η2) in the switch II region (Fig. 2B). Overlay of the Rab9 structure with H-Ras and structures of other Rab homologues (Ypt7p, Rab3A, Rab5C, Rab6, and Rab11A) results in root mean square (rms) deviations of 1.0–1.5 Å. This value drops to 0.6–1.0 Å when only the central β-sheet (50 Cα atoms) is overlaid, owing to the conserved nature of the core region. Important variations in the switch regions and the CDRs distinguish the Rab9 structure from other Rab homologues and are described below.

3.3. Significance of a Rab9 dimer

The two Rab9 molecules in the asymmetric unit are connected by an intermolecular β-sheet (Fig. 1) via their switch I and switch II regions. The buried surface area is ca. 1200 $Å^2$ and displays a relatively large shape complementarity coefficient S_c of 0.82, where a value of 1.0 would indicate perfect shape complementarity [28]. Ten hydrogen bonds and 137 van der Waals interactions are present in the interface. The buried surface area is inside the range observed for soluble protein/protein complexes of 1600 ± 400 $Å^2$ [29], opening the possibility of Rab9 forming dimers also in solution. Gel filtration studies both in near-physiological buffer (20 mM HEPES/NaOH, pH 7.4, and 150 mM NaCl) and in the crystallization medium clearly demonstrated Rab9 to be mono-disperse and to occur as a monomer (data not shown). Thus, the Rab9 dimer present in the crystal may either represent a fortuitous assembly or a biologically important low-affinity interaction. Similarly, the functionally related Rab11a forms a dimer by interaction of the switch I and switch II regions that buries ca. 2000 $Å^2$ of surface area, but is also monomeric in solution [30]. This corroborates the fact that there is no simple correlation of the extent of the buried surface area and complex stability [29,31]. Rather, tight complex formation is also dependent on the number of interactions and the complementarity of the interacting surfaces [32,33], which is quite high for the Rab9 dimer ($S_c = 0.82$) but comparatively low ($S_c = 0.63$) for the Rab11a dimer. Thus, dimers could form in vivo at endosomal membranes, where lateral diffusion increases the local concentration of Rab9, favoring low affinity interactions.

Comparison of the Rab9 and Rab11a complexes reveals very different relative orientations of the monomers: while in Rab9 the C-termini of the monomers point into opposing directions, in Rab11a they are located on the same side of the dimer. Both dimers could, however, attach to endosomal membranes because the flexible C-terminal part is long enough in either orientation to span the distance from the G-domain to the membrane. The burial of switch regions in a dimeric Rab complex may prevent binding of RabGDI [30,34,35]. Thus, a possible common function of the dimeric GDP-forms of Rab9 and Rab11a may be the generation of a pool of inactive Rab by dimerization at endosomal membranes. A timer function for vesicle fusion has been suggested for the Rab5 GTPase [36], which can undergo futile GTP/GDP hydrolysis cycles while attached to the membrane. While dimer formation has not been established in the Rab5 case, a similar timing function may be envisioned for the Rab9 and Rab11a dimers. Dimers have also been observed for the Rho family members Cdc42, Rac2, and RhoA [37]. Cdc42 and Rac2 form dimers in solution that display increased intrinsic GTPase activity, which was speculated to constitute a mechanism for negative regulation of these GTPases [37]. It appears that dimer formation of Ras-like GTPases may be more common than previously assumed and that these dimers may add to the arsenal of regulatory mechanisms of G proteins.

3.4. Metal ion coordination

Striking differences are apparent between the Rab9 molecules with respect to the metal ion coordination in the nucleotide binding site. Molecule B exhibits the classical octahedral coordination of Mg^{2+} with three water molecules and the hydroxyl group of Ser21 as the equatorial and the β-phosphate and a fourth water molecule as the apical ligands (Fig. 3B). By contrast, in molecule A a Sr^{2+} ion is observed for the first time in a Ras-like GTPase. Sr^{2+} is coordinated in a distorted pentagonal bipyramid by two oxygen atoms of the β-phosphate, the hydroxyl group of Ser21, three water molecules, and one benzoate ion in a bidentate fashion (Fig. 3A).

Mg^{2+} is an essential cofactor for GTP hydrolysis catalyzed by Ras-like GTP-binding proteins. Yet, other metal ions such as Mn^{2+} have also been found to bind to both the GDP- and the GTP-forms of the GTPases, Ras and Ran, and to significantly alter their structure and biochemical properties [38]. While Mg^{2+} and Mn^{2+} share similar ionic radii and are both hard ions with an octahedral coordination, it comes as a surprise that soft metals with larger ionic radii such as Sr^{2+} can substitute for Mg^{2+}. In the cases of Rab11a · GDP [30], RhoA [39], and Cdc42 · $GDPNH_2$ [27], a metal ion was even dispensable for maintaining structural integrity of the nucleotide-binding site. Normally, the affinity of Mg^{2+} for Ras-like GTPases is high with K_d values in the nanomolar or micromolar range [40,41] and removal of the metal ion destabilizes the GTPase · nucleotide complex [42–44]. In Rab11a, this destabilization is counteracted by a conformational change of the switch I region, while in RhoA switch I is stabilized by extensive crystal contacts. Taken together, the extreme

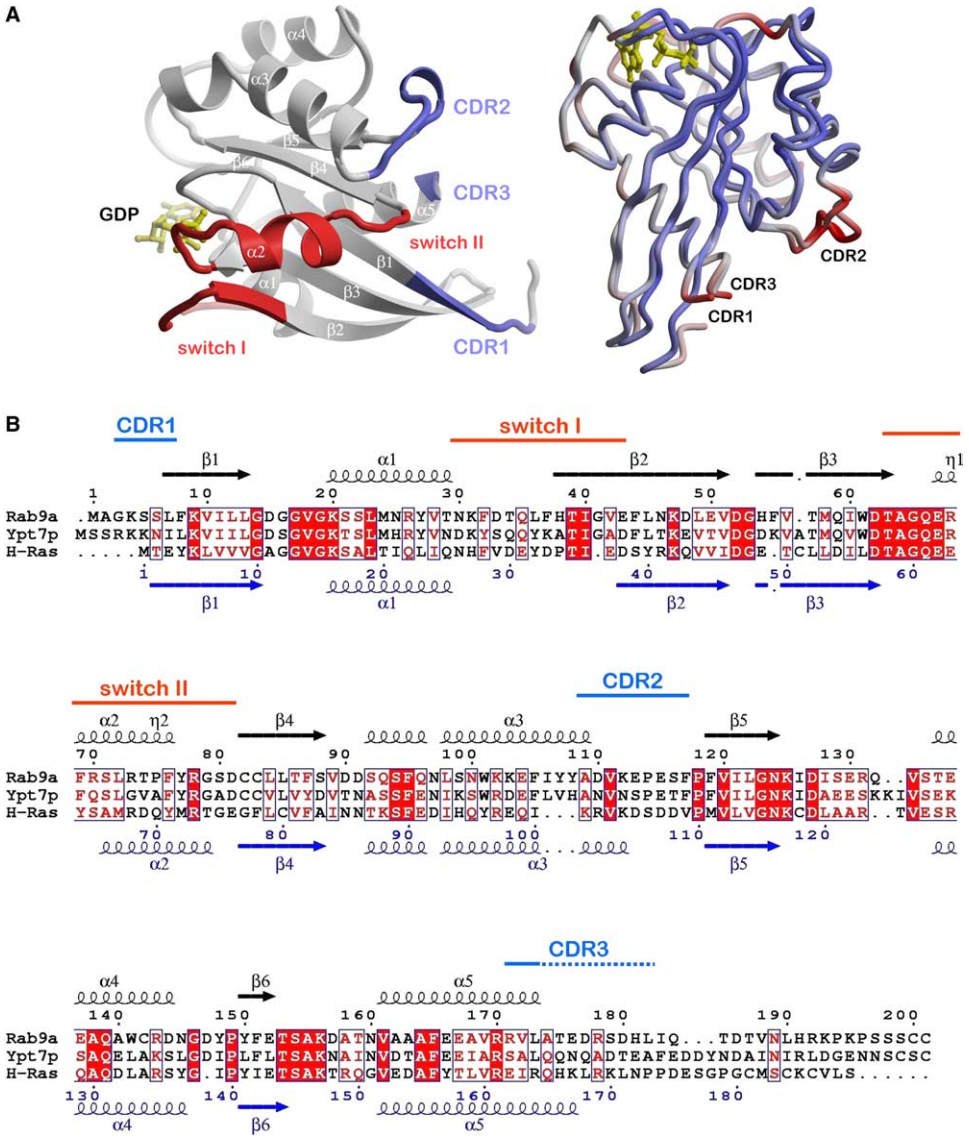

Fig. 2. Structure–sequence relationship of Rab9. (A) Left: Cα trace representation of molecule B of Rab9 with the switch regions and CDRs colored in red and blue, respectively. Right: Overlay of the two Rab molecules. Both molecules are colored according to increasing temperature factors from blue via gray to red, showing that the switch regions and CDRs display increased mobility. (B) The sequence alignment of Rab9 with the related Rab GTPase Ypt7p and H-Ras is shown with the secondary structure elements of Rab9 indicated in black on top and that for Ras in blue at the bottom. Conserved residues are highlighted by a red background and homologous residues are shown in red on a white background. This figure was prepared with ESPript [51].

variability in the presence, the nature, and the coordination of the metal ion demonstrates that the nucleotide binding pocket of Ras-like GTPases displays striking structural plasticity in the GDP-form.

3.5. *An active conformation of switch II in the GDP-bound state of Rab9*

With the exception of residues Val42 and Glu43 in molecule A, the switch I (Asn30–Glu43) and switch II (Thr63–Asp81) regions are ordered in the Rab9 structure. Rare cases of ordered switch regions are found in Cdc42 · GDP [27] and Rab11a · GDP [30]. Due to the lack of the γ-phosphate group, the switch regions are often more flexible in the GDP-form compared to the GTP-form of Ras-like GTPases. The unusually ordered switch regions in Rab9 · GDP are readily explained by the formation of the Rab9 dimer. Stabilizing interactions are contributed by an intermolecular antiparallel β-sheet formed by a large part of the switch I region, which results in an elongation of β-strand β2 (Fig. 2B). Both switch I regions share similar conformations but are further detached from the nucleotide binding pocket compared to Ras · GDP, Rab6 · GDP, and Rab11a · GDP. The switch II regions divert strongly from each other, displaying Cα–Cα distances of equivalent residues exceeding 5 Å (Fig. 4A). This conformational variability may help interaction of Rab/Ypt proteins with promiscuous Rab-binding proteins such as RabGDI [45].

Interestingly, the backbone trace of the switch II region in the Sr^{2+}-bound Rab9 molecule A is extremely similar to that of active, GppNHp-bound Rab3A [46] and Rab5C [47]. The crystal structure of the Rab3A/Rabphilin complex revealed a

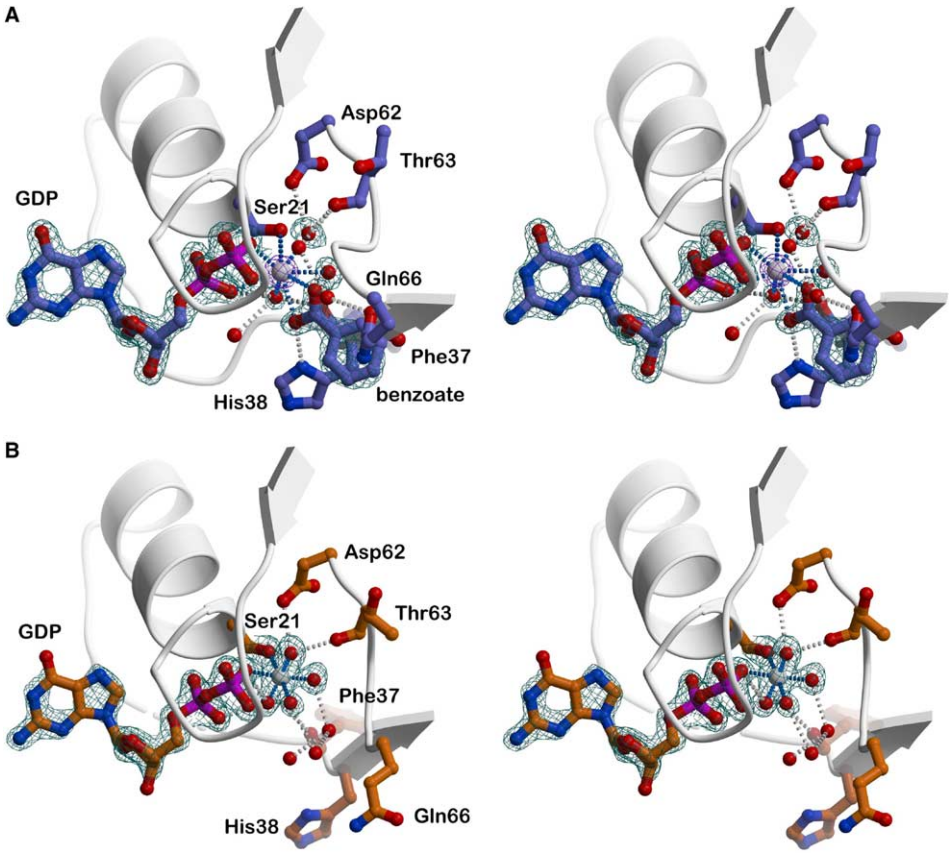

Fig. 3. Stereo representation of the electron density quality of the nucleotides from molecules A and B. The nucleotide is drawn as a stick model, water oxygen atoms are shown as red spheres, and the metal ions are depicted as gray spheres. The σ_A-weighted $2F_o - F_c$ electron density maps are contoured in blue at 1.8σ with the exception of the map for the Sr^{2+} ion, which is contoured in lilac at 10σ. The backbone of parts of the Rab9 protein, including the α_1-helix, the switch I region, and a part of the switch II region are shown in gray. (A) The Sr^{2+}-bound molecule A displays a distorted pentagonal bipyramidal coordination sphere with a total of eight interactions. (B) The Mg^{2+}-bound molecule B displays the canonical octahedral coordination.

conserved hydrophobic triad in Rab3A to form a Rabphilin-binding epitope [48]. This triad (Rab3A residues Phe59, Trp76, and Tyr91) is constructed by the active conformations of switch I and switch II. The corresponding residues in Rab9 (Phe44, Trp61, and Phe76) are similarly arranged with the aromatic side-chains stacking on top of each other. In addition, Pro75 contributes additional interactions by packing against Phe76, extending this hydrophobic motif into a tetrad (Fig. 4B). Thus, an effector-binding epitope is already present in one of the Rab9 · GDP structures. By contrast, although these residues are conserved in the closely related Rab7 homologue Ypt7p, the hydrophobic tetrad is absent in Ypt7p · GDP [15] because the switch regions are disordered. This fact further strengthens the argument that in the Sr^{2+}-bound Rab9 · GDP structure, the hydrophobic tetrad indeed is a structural mimicry for a conformation capable of effector binding.

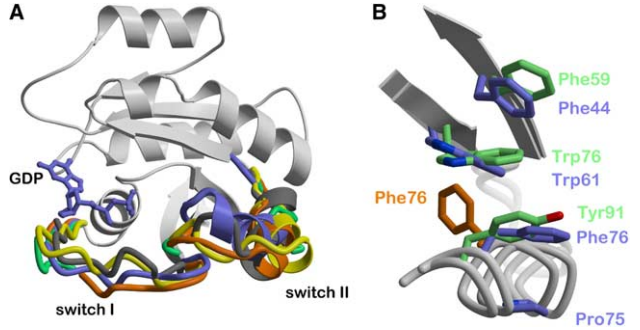

Fig. 4. Switch regions in Rab structures. (A) Overlay of the switch regions of GDP-bound Rab9 (blue for molecule A and orange for molecule B), Ypt7p (green), Rab11 (yellow), and Ras (gray). Only the ribbon model for Rab9 is shown in light gray for clarity. (B) The effector-binding epitope formed by the switch regions in the GppNHp-bound Rab3A structure is very similar to that present in the GDP-bound Rab9 structure. The Rab3A hydrophobic triad is shown in green, and the residues forming the hydrophobic tetrad in molecule A of Rab9 are drawn in blue. The epitope is not present in molecule B of Rab9 due to the rotation of Phe76 (orange) away from the surface towards the interior of the protein.

What is remarkable is that the Sr^{2+} ion, together with its benzoate ligand, drives the switch II region into a conformation that resembles that of the activated, GTP-bound Rab GTPases Rab3A [46] and Rab5C [47]. The carboxylate group of the benzoate falls close to the position of the γ-phosphate in Rab3A · GppNHp and Rab5C · GppNHp. A steric clash would result with conserved Gly65 of the DxxG motif if the switch II conformation remained unaltered. The clash is avoided by a shift of the entire switch II region of up to 6.5 Å (Cα atoms of Gly65) away from the nucleotide. As a result, the switch II region adopts an activated conformation, and even

the catalytically important glutamine side-chain (Gln61 in Ras, Gln66 in Rab9) is close to the position it adopts in GTP-bound Rabs (Fig. 3A). Furthermore, the size and shape of this epitope obviously vary with sequence such that it contains information on both the nucleotide state as well as the identity of the GTPase, providing an additional mechanism for Rab proteins for effector discrimination.

3.6. Morphology of the CDRs

While some of the Rab regulators such as REP and RabGDI show promiscuity for Rab proteins, others are highly specific for their respective Rab homologue. This specificity is due to sequence motifs named RabF and RabSF [49] that are used to classify Rab proteins into ten sub-families. The crystal structure of the Rab3A/Rabphilin complex [48] has delineated three CDRs [6] that overlap with the RabSF motifs found by sequence analysis. The CDRs are thought to confer binding specificity after initial interaction of the Rab effector with the switch regions. Comparison of the GDP- and GTP-forms of the related Rab homologue Rab11a reveals the CDR loop structures to be very similar and, thus, nucleotide-independent. There is apparently no signal transduction from the nucleotide binding pocket across the G domain to the CDR loops, enabling meaningful comparison of these regions also in GDP-bound Rab structures.

A continuous three-dimensional epitope is formed by CDR1, CDR2, and CDR3 (Fig. 2A) with CDR1 and CDR3 located at the N- and C-terminus, respectively, and CDR2 encompassing the α3/β5 loop. Most components of this epitope are ordered in the Rab9 structure and they display elevated temperature factors compared to the body of the G domain. Having no restraints from crystal packing, CDR2 in molecule A is only partially defined by electron density and CDR2 in molecule B adopts a unique conformation not seen in other Rab structures and also with respect to the GDP- and GppNHp-bound structures of Ypt7p (Figs. 5A and B). The comparison with Ypt7p is particularly interesting given the high overall sequence homology (58%) and their related functions: yeast Ypt7p is involved in endosome to vacuole trafficking [50], while Rab9 is a key regulator of endosome to Golgi trafficking [7]. CDR2 in Rab9 and also in Ypt7p contains a four residue insertion compared to other Rabs (Fig. 5C), rendering this loop inherently more flexible. Similar to the switch regions, CDR2 in Rab9 and Ypt7p will become fixed only upon effector binding. Thus, a first means of effector discrimination seems to be the length of CDR2. Further selection must then be achieved by sequence differences in the CDR2 regions, which is indeed the case (Fig. 5B). It can therefore be expected that CDR2 is a major discriminating epitope in complexes of Rabs with their effector.

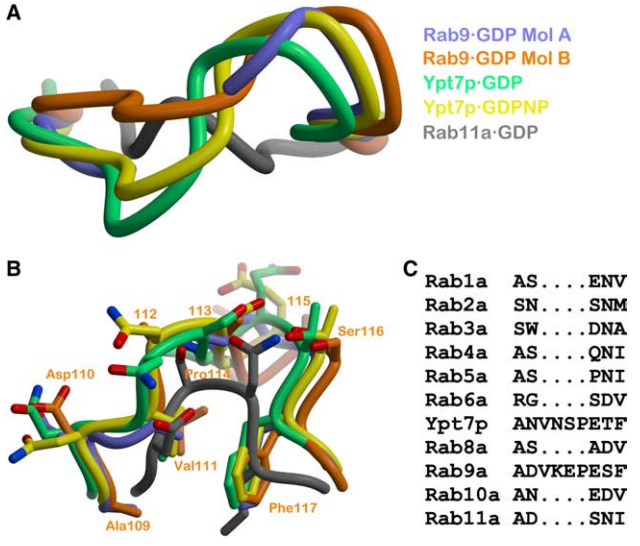

Fig. 5. Structural variability of the CDR2 (α3/β5) loop. (A) Top view of the Cα traces of the CDR2 region for Rab9 (blue for molecule A and orange for molecule B), Ypt7p (green for the GDP-form and yellow for the GppNHp-form), and Rab11 (gray). (B) Side view of (A) rotated by 90° around the *x*-axis with side-chains drawn as stick models with the same color code as in (A). (C) Sequence alignment of the CDR2 region of Rab proteins showing the four amino acid insertion in Rab9 and Ypt7.

Acknowledgements: We thank Andrea Schmidt and Victor Lamzin at DESY beamline BW7A for guidance during synchrotron data collection, Suzanne Pfeffer for providing Rab9 cDNA, Ralf Ficner for generous support throughout the project, and Dagmar Klostermeier for critically reading the manuscript. This study was supported by a grant from the DFG (SFB523) to MGR. The coordinates and structure factors of Rab9·GDP have been deposited in the Protein Data Bank under ID code 1S8F.

References

[1] Block, M.R., Glick, B.S., Wilcox, C.A., Wieland, F.T. and Rothman, J.E. (1988) Proc. Natl. Acad. Sci. USA 85, 7852–7856.
[2] Rothman, J.E. (1994) Nature 372, 55–63.
[3] Bourne, H.R., Sanders, D.A. and McCormick, F. (1990) Nature 348, 125–132.
[4] Scheffzek, K., Ahmadian, M.R. and Wittinghofer, A. (1998) Trends Biochem. Sci. 23, 257–262.
[5] Pfeffer, S.R. (2001) Trends Cell Biol. 11, 487–491.
[6] Moyer, B.D. and Balch, W.E. (2001) Methods Enzymol. 329, 3–6.
[7] Lombardi, D., Soldati, T., Riederer, M.A., Goda, Y., Zerial, M. and Pfeffer, S.R. (1993) EMBO J. 12, 677–682.
[8] Dell'Angelica, E.C., Puertollano, R., Mullins, C., Aguilar, R.C., Vargas, J.D., Hartnell, L.M. and Bonifacino, J.S. (2000) J. Cell Biol. 149, 81–94.
[9] Robinson, M.S. and Bonifacino, J.S. (2001) Curr. Opin. Cell Biol. 13, 444–453.
[10] Diaz, E. and Pfeffer, S.R. (1998) Cell 93, 433–443.
[11] Bonifacino, J.S. (2004) Nat. Rev. Mol. Cell. Biol. 5, 23–32.
[12] Wittmann, J.G. and Rudolph, M.G. (2004) Acta Cryst. D 60, 580–582.
[13] Otwinowski, Z. and Minor, W. (1997) Methods Enzymol. 276, 307–326.
[14] Jogl, G., Tao, X., Xu, Y. and Tong, L. (2001) Acta Cryst. D 57, 1127–1134.
[15] Constantinescu, A.T., Rak, A., Alexandrov, K., Esters, H., Goody, R.S. and Scheidig, A.J. (2002) Structure 10, 569–579.
[16] CCP4 (1994) Acta Cryst. D 50, 760–763.
[17] Read, R.J. (1986) Acta Cryst. A 42, 140–149.
[18] Jones, T.A., Cowan, S., Zou, J.Y. and Kjeldgaard, M. (1991) Acta Cryst. A 47, 110–119.
[19] Brünger, A.T. et al. (1998) Acta Cryst. D 54, 905–921.
[20] Sheldrick, G.M. and Schneider, T.R. (1997) Methods Enzymol. 277, 319–343.
[21] Brünger, A.T. (1992) Nature 355, 472–475.
[22] McDonald, I.K. and Thornton, J.M. (1994) J. Mol. Biol. 238, 777–793.
[23] Laskowski, R.A., MacArthur, M.W., Moss, D.S. and Thornton, J.M. (1993) J. Appl. Cryst. 26, 283–291.
[24] Hooft, R.W., Vriend, G., Sander, C. and Abola, E.E. (1996) Nature 381, 272.
[25] Esnouf, R.M. (1997) J. Mol. Graph. 15, 132–134.

[26] Merritt, E.A. and Murphy, M.E.P. (1994) Acta Cryst. D 50, 869–873.
[27] Rudolph, M.G., Wittinghofer, A. and Vetter, I.R. (1999) Prot. Sci. 8, 778–787.
[28] Lawrence, M.C. and Colman, P.M. (1993) J. Mol. Biol. 234, 946–950.
[29] Lo Conte, L., Chothia, C. and Janin, J. (1999) J. Mol. Biol. 285, 2177–2198.
[30] Pasqualato, S., Senic-Matuglia, F., Renault, L., Goud, B., Salamero, J. and Cherfils, J. (2004) J. Biol. Chem. 279, 11480–14488.
[31] Rudolph, M.G., Linnemann, T., Grunewald, P., Wittinghofer, A., Vetter, I.R. and Herrmann, C. (2001) J. Biol. Chem. 276, 23914–23921.
[32] Garcia, K.C. (1999) Immunol. Rev. 172, 73–85.
[33] Rudolph, M.G. and Wilson, I.A. (2002) Curr. Opin. Immunol. 14, 52–65.
[34] Beranger, F., Cadwallader, K., Porfiri, E., Powers, S., Evans, T., de Gunzburg, J. and Hancock, J.F. (1994) J. Biol. Chem. 269, 13637–13643.
[35] Rak, A. et al. (2003) Science 302, 646–650.
[36] Rybin, V., Ullrich, O., Rubino, M., Alexandrov, K., Simon, I., Seabra, M.C., Goody, R. and Zerial, M. (1996) Nature 383, 266–269.
[37] Zhang, B. and Zheng, Y. (1998) J. Biol. Chem. 273, 25728–25733.
[38] Schweins, T., Scheffzek, K., Assheuer, R. and Wittinghofer, A. (1997) J. Mol. Biol. 266, 847–856.
[39] Shimizu, T., Ihara, K., Maesaki, R., Kuroda, S., Kaibuchi, K. and Hakoshima, T. (2000) J. Biol. Chem. 275, 18311–18317.
[40] John, J., Rensland, H., Schlichting, I., Vetter, I., Borasio, G.D., Goody, R.S. and Wittinghofer, A. (1993) J. Biol. Chem. 268, 923–929.
[41] Simon, I., Zerial, M. and Goody, R.S. (1996) J. Biol. Chem. 271, 20470–20478.
[42] Tucker, J., Sczakiel, G., Feuerstein, J., John, J., Goody, R.S. and Wittinghofer, A. (1986) EMBO J. 5, 1351–1358.
[43] Hall, A. and Self, A.J. (1986) J. Biol. Chem. 261, 10963–10965.
[44] John, J., Frech, M. and Wittinghofer, A. (1988) J. Biol. Chem. 263, 11792–11799.
[45] Garrett, M.D., Zahner, J.E., Cheney, C.M. and Novick, P.J. (1994) EMBO J. 13, 1718–1728.
[46] Dumas, J.J., Zhu, Z., Connolly, J.L. and Lambright, D.G. (1999) Structure Fold. Des. 7, 413–423.
[47] Merithew, E., Hatherly, S., Dumas, J.J., Lawe, D.C., Heller-Harrison, R. and Lambright, D.G. (2001) J. Biol. Chem. 276, 13982–13988.
[48] Ostermeier, C. and Brunger, A.T. (1999) Cell 96, 363–374.
[49] Pereira-Leal, J.B. and Seabra, M.C. (2000) J. Mol. Biol. 301, 1077–1087.
[50] Wichmann, H., Hengst, L. and Gallwitz, D. (1992) Cell 71, 1131–1142.
[51] Gouet, P., Courcelle, E., Stuart, D.I. and Metoz, F. (1999) Bioinformatics 15, 305–308.
[52] Luzzati, V. (1952) Acta Cryst. 5, 802–810.